Olivine intergranular plasticity at mantle pressures and temperatures

Paul Raterron, Caroline Bollinger, Sébastien Merkel

Olivine intergranular plasticity at mantle pressures and temperatures

Paul Raterron*, Caroline Bollinger[†], Sébastien Merkel

Unité Matériaux et Transformation (UMET), CNRS, Université Lille 1, F-59655 Villeneuve d'Ascq Cedex, France.

*Corresponding author, presently at National Science Foundation, 2415 Eisenhower Avenue, Alexandria, VA 22314, USA; praterro@nsf.gov

[†] Now at: Bayerisches Geoinstitut, University of Bayreuth, 95440 Bayreuth, Germany

Key points:

We quantify the strain accommodated by grain-to-grain interactions in olivine aggregates.

Our results demonstrate that intergranular plasticity is dominant at mantle pressure.

Olivine strength in the mantle may be lower than predicted by classical flow laws.

Abstract

The ductile behavior of olivine-rich rocks is critical to constrain thermal convection in the Earth's upper mantle. Classical olivine flow laws for dislocation or diffusion creep fail to explain the fast post-seismic surface displacements observed by GPS, which requires a much weaker lithosphere than predicted by classical laws. Here we compare the plasticity of olivine aggregates deformed experimentally at mantle pressures and temperatures to that of single crystals and demonstrate that, depending on conditions of stress and temperature, strain accommodated through grain-to-grain interactions - here called intergranular strain - can be orders of magnitude larger than intracrystalline strain, which significantly weakens olivine strength. This result, extrapolated along mantle geotherms suggests that intergranular plasticity could be dominant in most of the upper mantle. Consequently, the strength of olivine-rich aggregates in the upper mantle may be significantly lower than predicted by flow laws based on intracrystalline plasticity models.

1. Introduction

The plasticity of olivine-rich rocks constraints that of Earth's upper mantle. Consequently, there has been considerable effort to quantify olivine aggregate rheology in terms of flow laws which can be implemented in geodynamical models for mantle thermal convection. Experimental studies investigated the effects of temperature and stress [a review in *Hirth and Kohlstedt*, 2003], pressure [e.g., *Durham et al.*, 2009; *Hilairet et al.*, 2012; *Bollinger et al.*, 2013], fluid fugacities [e.g., *Kohlstedt*, 2006; *Keefner et al.*, 2011; *Ohuchi at al.*, 2017], grain size [*Warren and Hirth*, 2006], lattice preferred orientations [e.g., *Hansen et al.*, 2013] and melt fractions [e.g., *Hirth and Kohlstedt*, 1995]. The traditional view is to assign one dominant deformation mechanism to given deformation conditions [*Frost and Ashby*, 1982] and implement the flow law with specific dependences on temperature, stress or grain size. At the microscopic scale, however, olivine aggregate plasticity involves numerous mechanisms operating concurrently, within the grains and at grain boundary (Fig. 1). To this day, the fundamental question of the amount of strain accommodated in the mantle through grain-to-grain interactions versus that accommodated within the grain remains unanswered.

Strain accommodation at grain boundary has been attributed to several distinct mechanisms. A model for the deformation of aggregates by grain-boundary diffusion was introduced by *Coble* [1963] to explain the high-temperature plasticity of alumina. Coble creep requires the rearrangement of grain interfaces by grain-boundary sliding (GBS). The corresponding flow law exhibits a linear dependence on stress and a strong inverse dependence on grain size (d), theoretically to the power $p = -3$. For persistently small grain sizes - when grain growth is for example impeded by Zener pinning - Coble creep may contribute to superplastic flow, which has been characterized at room pressure in olivine rich aggregates [e.g., *Hiraga et al.*, 2010]. Grain-boundary sliding can also be assisted by dislocation motions within grains, which contribute to relax stress concentration at triple

53 junctions. This mechanism, called dislocation-assisted grain boundary sliding (disGBS), has
54 been observed at low pressure in olivine [*Hirth and Kohlstedt*, 2003; *Hansen et al.*, 2011]. It
55 is characterized by a strain rate depending strongly on stress, typically to the power $n \sim 3$,
56 with an inverse dependence on grain size to a power p within [-2, -0.6]. Other deformation
57 mechanisms, which do not exist in single crystals, accommodate strain in olivine aggregates.
58 Motions of disclinations - defects identified along grain boundaries in olivine [*Cordier et al.*,
59 2014] - can accommodate strain. Furthermore, interactions between grains, in materials with
60 limited number of intracrystalline deformation mechanisms, generate locally high stress
61 concentration [e.g., *Castelnau et al.*, 2008]. In materials with anisotropic elastic and plastic
62 properties such as olivine this may promote high stress and strain transmission patterns
63 percolating throughout the aggregates [*Burnley*, 2013]. Conversely, the stress field associated
64 with single-crystal deformation can only be relaxed by intracrystalline deformation
65 mechanisms, such as dislocation motions (glide, climb and cross slip) and intracrystalline
66 diffusion (e.g., Nabarro-Herring diffusion).

67 Recently, *Tielke et al.* [2016] compared olivine single-crystal and aggregate high-
68 temperature rheology at low pressure, and quantified the contribution of both intracrystalline
69 and intergranular mechanisms to the aggregate strain. They determine that olivine aggregates
70 deform up to 4.6 times faster than what would be expected assuming only intracrystalline
71 plasticity; the latter's contribution to strain rate was calculated from micromechanical
72 modeling of dislocations activity. Following a similar approach, we here compare olivine
73 single-crystal and aggregate high-temperature plasticity, as measured experimentally at the
74 high pressures representative of mantle conditions. We demonstrate that grain-to-grain
75 interactions significantly contribute to accommodating strain in experiments. Extrapolation to
76 mantle stress conditions along geotherms suggests that intergranular plasticity may also
77 dominate upper mantle plasticity.

2. Methods: intracrystalline vs intergranular plasticity

Comparing aggregates and single-crystal deformation data allows quantifying the strain rate contributions of intergranular deformation mechanisms. Assuming that intracrystalline (IC) and intergranular (IG) mechanisms operate concurrently, we have:

$$\dot{\varepsilon}_{\mathrm{Agg}} = \dot{\varepsilon}_{\mathrm{IC}} + \dot{\varepsilon}_{\mathrm{IG}} \qquad (1),$$

where $\dot{\varepsilon}_{\mathrm{Agg}}$ is the strain rate of the aggregate, $\dot{\varepsilon}_{\mathrm{IC}}$ is the contribution of intracrystalline processes and $\dot{\varepsilon}_{\mathrm{IG}}$ is due to grain-to-grain interactions. The plasticity of aggregates can thus be quantified by introducing the following ratio:

$$\dot{\varepsilon}_{\mathrm{Agg}}/\dot{\varepsilon}_{\mathrm{IC}} = 1 + \dot{\varepsilon}_{\mathrm{IG}}/\dot{\varepsilon}_{\mathrm{IC}} \qquad (2),$$

It should range from 1, when all the aggregate strain is accommodated within the grains, to $+\infty$, when the strain is fully accommodated through grain-to-grain deformation processes. Values for $\dot{\varepsilon}_{\mathrm{Agg}}$ and $\dot{\varepsilon}_{\mathrm{IC}}$ (and their ratio $\dot{\varepsilon}_{\mathrm{Agg}}/\dot{\varepsilon}_{\mathrm{IC}}$) can be directly extracted from previously published rheological data (Figure 2).

We used $\dot{\varepsilon}_{\mathrm{Agg}}$ values for San Carlos olivine aggregates deformed in axisymmetric compression at mantle pressure and temperature in the Deformation-DIA (D-DIA) apparatus, as reported by *Durham et al.* [2009], *Hilairet et al.* [2012] and *Bollinger et al.* [2013] (supplementary Table S1). For each $\dot{\varepsilon}_{\mathrm{Agg}}$ reported value, the corresponding $\dot{\varepsilon}_{\mathrm{IC}}$ can be calculated at identical pressure (P), temperature (T) and differential stress (σ) by combining experimental flow laws for San Carlos olivine single crystals [*Mackwell et al.*, 1985; *Bai et al.*, 1991, *Raterron et al.*, 2009, 2012; *Girard et al.*, 2013] (supplementary materials, Table S2). Indeed, assuming homogeneous stress throughout the aggregate (lower bound approach,

100 i.e. Sachs' bound) - one of the simplest end-member assumption when analytically addressing
101 aggregate strain - and random grain orientations in the aggregate, $\dot{\varepsilon}_{IC}$ reads:

102 $$\dot{\varepsilon}_{IC} = 0.123\ (\dot{\varepsilon}_{[110]c} + \dot{\varepsilon}_{[011]c} + \dot{\varepsilon}_{[101]c}) \qquad (3),$$

103 where $\dot{\varepsilon}_{[110]c}$, $\dot{\varepsilon}_{[011]c}$, and $\dot{\varepsilon}_{[101]c}$ are the strain rates of oriented single crystals and the
104 0.123 geometrical factor arises from averaging over crystal orientations [*Raterron et al.*,
105 2011]. The indexes indicate the crystallographic orientation of the compression direction –
106 e.g., $[110]_c$ direction is at 45° angle from [100] and [010] directions. $[110]_c$, $[011]_c$, $[101]_c$
107 promote respectively [100](010) dislocation slip, [001](010) dislocation slip, and [100](001)
108 and [001](100) slips together. The single-crystal strain rates $\dot{\varepsilon}_{[110]c}$, $\dot{\varepsilon}_{[011]c}$, and $\dot{\varepsilon}_{[101]c}$
109 account for pressure, temperature, water content, and oxygen fugacity (fO_2) and are based on
110 data from the literature (Supplementary information). For the dry experiments reported by
111 *Durham et al.* [2009] (squares in Fig. 2), we assumed a dry-crystal rheology when calculating
112 $\dot{\varepsilon}_{IC}$; for the wet experiments reported by *Hilairet et al.* [2012] and *Bollinger et al.* [2013]
113 (triangles and circles in Fig. 2), we assumed wet-crystal rheology. $\dot{\varepsilon}_{IC}$ was also calculated
114 assuming oxygen fugacity conditions comparable to those of the experiments. For *Durham et*
115 *al.'s* [2009] experiments, where the Ni/NiO buffer controlled fO_2, we assumed the Ni/NiO
116 buffer oxygen fugacity [*Frost*, 1991]. For the unbuffered experiments [*Hilairet et al.*, 2012;
117 *Bollinger et al.*, 2013] - where oxygen fugacity was not controlled but specimens were placed
118 within a boron nitride sleeve which promotes low fO_2 conditions [*Wendland et al.*, 1985] - we
119 assumed the oxygen fugacity of the iron-wüstite buffer (IW) which borders the olivine
120 stability field.

121 **3. Results: aggregate strain rate $\dot{\varepsilon}_{Agg}$ versus intracrystalline strain rate $\dot{\varepsilon}_{IC}$**

122 Figure 2.a shows the aggregate strain rate $\dot{\varepsilon}_{Agg}$, as measured experimentally (Table
123 S1), versus the intracrystalline strain rate $\dot{\varepsilon}_{IC}$ (Eq. 3) calculated at identical P, T and σ.

Because of our initial assumption (Sachs' bound), Eq. 3 tends to overestimate the intracrystalline strain rate. This may occasionally lead to $\dot{\varepsilon}_{Agg} < \dot{\varepsilon}_{IC}$ when strain is fully accommodated by intracrystalline processes. Remarkably, we have $\dot{\varepsilon}_{Agg} \geq \dot{\varepsilon}_{IC}$ (within uncertainty) for all but one experimental point, by factors reaching ~20 at 1673 K and ~2000 at 1373 K. This shows that, in high-pressure deformation experiments, *i)* a significant fraction of aggregate strain is accommodated by mechanisms involving grain-to-grain interactions, even in regimes where dislocation creep was observed. It also shows that *ii)* this fraction tends to increase with decreasing temperature. Also show on Figure 2.a are the data reported by Tielke el al. (2016) obtained at low pressure (open diamonds, green is for 1523 K). For these data, shear strain rates and stresses were converted into compressional strain rates and stresses before plotting. Tielke et al. report that the aggregate strain rate is up to 4.6 times higher than the intracrystalline strain rate as calculated using a micromechanical modeling; Figure 2.a shows that these data fall, indeed, in the vicinity of the line corresponding to a ratio of 4.6 between the measured strain rate and the intracrystalline strain rates calculated here using the analytical approach described above. It is remarkable that using two different approaches, Tielke et al. and we obtained similar results. This give us confidence in the analytical approach used here.

Figure 2.b shows $\log(\dot{\varepsilon}_{Agg}/\dot{\varepsilon}_{IC})$ versus stress; the color code indicate approximate temperatures. The ratio $\dot{\varepsilon}_{Agg}/\dot{\varepsilon}_{IC}$ varies over orders of magnitude, from ~ 1 to ~2×10^3. When $\dot{\varepsilon}_{Agg}/\dot{\varepsilon}_{IC} \sim 1$ the aggregate strain is fully accommodated within the grains, while $\dot{\varepsilon}_{Agg}/\dot{\varepsilon}_{IC} \gg 2$ indicates that strain is mostly accommodated by grain-to-grain interactions (intergranular mechanisms). Within our model, one should always satisfy $\dot{\varepsilon}_{Agg}/\dot{\varepsilon}_{IC} \geq 1$ (Eq. 2) which, within uncertainties, is in agreement with most experimental data. At a given temperature, $\log(\dot{\varepsilon}_{Agg}/\dot{\varepsilon}_{IC})$ decreases with increasing differential stress (Fig. 2.b) until $\log(\dot{\varepsilon}_{Agg}/\dot{\varepsilon}_{IC}) \sim 0$

148 is achieved, i.e. strain is fully accommodated within the grains ($\dot{\varepsilon}_{Agg} = \dot{\varepsilon}_{IC}$). A further
149 increase of stress will have no effect on Eq. 2 ratios. This result is in agreement with the
150 conventional interpretation that increasing stress and strain rate at given temperature favors
151 dislocation creep [*Frost and Ashby*, 1982] - a grain-size insensitive creep involving mostly
152 intracrystalline plasticity - with respect to grain-size sensitive creep which involves
153 intergranular plasticity.

154 The contribution of grain-to-grain deformation processes to the aggregate strain also
155 decreases with temperature (Figs. 2a and 2.b). This effect may result from a combination of
156 factors, such as: an increasing aggregate grain size with temperature, i.e., a decreasing grain-
157 boundary surface/bulk volume ratio favoring intracrystalline deformation mechanisms; an
158 increasing activity of disclinations with decreasing *T* favoring intergranular plasticity; higher
159 stress and strain concentrations near grain boundaries at lower *T,* or a more effective stress
160 percolation at moderate *T* [*Burnley*, 2012] promoting high-strain networks throughout the
161 aggregates, accounted here for as intergranular strain.

162 A linear fit through $\log(\dot{\varepsilon}_{Agg}/\dot{\varepsilon}_{IC})$ in Figure 2.b leads to the empirical equation:

163 $$\log(\dot{\varepsilon}_{Agg}/\dot{\varepsilon}_{IC}) = 20.4 - 0.0115\,T - 0.0045\,\sigma \qquad (4),$$

164 where *T* is in K, and the differential stress σ is in MPa. $\dot{\varepsilon}_{Agg}/\dot{\varepsilon}_{IC}$ must remain ≥ 1. Therefore,
165 $\dot{\varepsilon}_{Agg}/\dot{\varepsilon}_{IC} = 1$ is here imposed when Eq. 4 gives values < 1. Note that, although empirical,
166 Eq. 4 accounts for all dry and wet data with good consistency between studies. Combining
167 Eqs. 2 and 4, a first-order estimate of olivine aggregate strain rate can be calculated from the
168 intracrystalline strain rate $\dot{\varepsilon}_{IC}$ (Eq. 3) through the following composite flow law:

169 $$\dot{\varepsilon}_{Agg} = \mathrm{Max}[1; 10\hat{}(20.4 - 0.0115\,T - 0.0045\,\sigma)] \times \dot{\varepsilon}_{IC} \qquad (5),$$

170 where Max[i; j] is the maximum of i and j , *T* is in K and σ is in MPa. Note that the effects of
171 pressure, temperature, stress, oxygen fugacity, or hydrous conditions are accounted for in the

intracrystalline flow laws (Eq. 3, supplementary materials, Table S2). In the following, we explore the implications for the upper mantle of the effect of pressure and temperature on intracrystalline vs intergranular plasticity.

4. Discussion: Extrapolation to mantle conditions

Figure 3.a shows $\log(\dot{\varepsilon}_{Agg}/\dot{\varepsilon}_{IC})$ calculated along two oceanic geotherms (20-Ma and 80-Ma) for a differential stress σ = 1 MPa - i.e., a shear stress $\mu = 1/\sqrt{3}$ MPa which is a reasonable value for the mid to deep upper mantle [*Bürgmann and Dresen*, 2008] - and along a classic continental geotherm (supplementary Fig. S1, see also *Turcotte and Schubert* [2002]) for σ = 1 and 50 MPa. The latter stress value is representative of shear zone in the coldest part of the lithosphere, and of experimental conditions. For this calculation, pressure was calculated with an upper-mantle average density of 3.35 g/cm^3 (i.e. a 32.9 MPa/km vertical pressure gradient), and oxygen fugacity set at FMQ-2 which is reasonable for the upper mantle [*Herd*, 2008]. We assumed wet condition for this plot (supplementary materials). Figure 3.a suggests that, like in experiments, deformation in the upper mantle is largely accommodated by intergranular plasticity, especially in the cold lithosphere where grain-to-grain interactions may fully dominate olivine plasticity. This may promote a significant weakening of the aggregate with respect to the strength calculated from classical flow laws.

Figures 3.b shows the viscosity of olivine aggregate along oceanic (20 Ma, red curves) and continental (blue curves) geotherms, as calculated using the composite flow law of Eq. 5 for a differential stress of 1 MPa. Wet conditions are assumed when using Eq. 5, as well as for plotting the *Hirth and Kohlstedt* [2003] dislocation creep flow law with hydroxyl content C_{OH} = 300 ppm H/Si. The intracrystalline strain rate calculated from Eq.3 is shown for comparison, together with two low-temperature flow laws [*Raterron et al.*, 2004; *Demouchy et al.*, 2013]. In both contexts, the composite flow law in Eq. 5 leads to viscosities about two

196 orders of magnitude lower that the *Hirth and Kohlstedt*'s dislocation creep flow law.
197 Interestingly, in the shallow (cold) upper mantle, the composite flow law of Equation 5 is in
198 relatively good agreement with the low-temperature flow laws reported for olivine, thus
199 captures the change in rheology between high-temperature and low-temperature plasticity.
200 Changing the differential stress to 50 MPa does not significantly affect these results
201 (Supplemental Figure S2). At deeper depths (i.e. 400 km), the difference between the
202 predictions of Eq. 5 and the dislocation creep law of *Hirth and Kohlstedt* [2003] is due to the
203 pressure-induced change of dominant slip system in olivine [*Raterron et al.*, 2012].

204 It should be emphasized here that polycristalline specimens in high-pressure experiments have
205 small grain sizes, typically ranging from 1 to 50 µm, which increases significantly their
206 surface versus volume ratio when compared to that of mantle rocks with estimated grain siz**es**
207 ranging from tenths of millimetre to centimetres. This enhances grain-to-grain interactions,
208 hence intergranular plasticity, in laboratory specimens and may artificially lower their
209 strenght with respect to that of mantle rocks. The results reported here (Eq. 5 and Fig. 2) may,
210 thus, significantly overestimate how much strain can be accomodated by grain-to-grain
211 interactions in the coarse-grain mantle. However, our results may apply more directly in the
212 context of mantle shear zones, where grain-size reduction weakens sheared peridotites
213 (Warren and Hirth, 2006; Skemer et al., 2011).

5. Concluding remarks

According to our results and extrapolation, we conclude that olivine strain is mostly accommodated by deformation mechanisms involving grain-to-grain interactions at mantle pressures and temperatures, which results in a much weaker strength as that obtained when combining single-crystal dislocation creep flow laws. Such a phenomenon was recently observed at low pressure [*Tielke et al.*, 2016], but is much more marked at high pressure where intergranular plasticity largely dominate deformation.

Uncertainties remain regarding the additional deformation mechanisms, present in aggregates and absent in single crystals, responsible for the measured low strength of aggregates with respect to that of single crystals. Several candidate mechanisms are mentioned in the introduction, such as disclinations, grain boundary sliding, stress/strain percolation, etc., but our analysis does not allow to favor one over another.

Furthermore, the empirical model presented here is extracted from deformation experiments carried out at high differential stresses on aggregates with small grain sizes compared to mantle conditions where stresses are much lower and grain sizes larger -. Further investigation is necessary to quantify the effects of increasing grain size and decreasing stress on Eq.4 parameters. As mentioned above, one may speculate that, due to the larger grain sizes, intracrystalline mechanisms may accommodate more strain in the Earth's mantle than in experiments and, hence, reduce the effect of grain-to-grain interactions highlighted here. Another source of discrepancy when extrapolating the present results to mantle processes is the presence of secondary phases such as pyroxenes, garnet and possibly partial melts in mantle peridotites which are absent in the present laboratory specimens.

Keeping in mind the above reservations, let us however emphasize that olivine classical flow laws, whether assuming dislocation or diffusion creep, fail to explain the fast surface displacement observed by GPS after large earthquakes [e.g., *Freed et al.*, 2010],

239 which requires a much weaker strength for the lithosphere, as the one we propose here. Also,
240 the particularly deep weakening predicted here along a continental geotherm may provide an
241 explanation for the elusiveness of the lithosphere-asthenosphere boundary beneath cratons
242 [e.g., Eaton et al., 2009], since it should reduce the lithosphere-asthenosphere viscosity
243 contrast. We thus conclude that grain-to-grain interactions are an important component of
244 olivine plasticity at mantle pressures, and may likely contribute to the weakening of the
245 Earth's upper mantle with respect to that calculated from classical flow laws for olivine.
246

247 **References**

248 Bai, Q., Mackwell, S.J., Kohlstedt, D.L. (1991) High-temperature creep of olivine single
249 crystals.1. Mechanical results for buffered samples, *Journal of Geophysical Research* **96**,
250 2441-2463.
251 Bollinger, C., Merkel, S., Raterron, P., Cordier, P. (2013) Olivine dislocation creep: revisiting
252 experimental data to 8 GPa pressure, *Phys. Earth Planet. Int.* **228**, 211-219.
253 Burnley, P.C. (2013) The importance of stress percolation patterns in rocks and other
254 polycrystalline materials, *Nature Communications* **4**:2117, doi: 10.1038/ncomms3117.
255 Bürgmann, R., Dresen, G. (2008) Rheology of the lower crust and upper mantle: evidence
256 from rock mechanics, geodesy and field observations. *Annu. Rev. Earth Planet. Sci.* **36**,
257 531–567.
258 Castelnau, O., Blackman, D.K., Lebensohn, R.A., Ponte Castañeda (2008) Micromechanical
259 modeling of viscoplastic behavior of olivine, J. Geophys. Res. 113, B09202,
260 doi:10.1029/2007JB005444.
261 Coble, R.L. (1963) A model for boundary diffusion controlled creep in polycrystalline
262 materials, *J. Appl. Physics* **34** (6), 1679-1682.
263 Cordier, P., Demouchy, S., Beausir, B., Taupin, V., Barou, F., Fressengeas, C. (2014)
264 Disclinations provide the missing mechanism for deforming olivine-rich rocks in the
265 mantle, *Nature* **504**, 51-56, doi:10.1038/nature13043.
266 Demouchy, S., Tommasi, A., Boffa Ballaran, T., Cordier, P. (2013) Low strength of Earth's
267 uppermost mantle inferred from tri-axial deformation experiments on dry olivine crystals,
268 *Physics of the Earth and Planetary Interiors* **220**, 37-49.
269 Durham, W.B., Mei, S., Kholstedt, D.L., Wang, L., Dixon, N.A. (2009) New measurement of
270 activation volume in olivine under anhydrous conditions*, Phys. Earth Planet. Int.* **172**, 67-
271 73.
272 Eaton, D.W., Darbtshire, F, Evans, R.L., Grütter, H., Jones, A.G., Yuan, X. (2009) The
273 elusive lithosphere-asthenosphere boundary (LAB) beneath cratons, *Lithos* **109**, 1-22.
274 Freed, A.M., Herring, T., Bürgmann, R. (2010) Steady-state laboratory flow laws alone fail to
275 explain postseismic observations, *Earth and Planetary Science Letters* **300**, 1-10.
276 Frost, H.J., Ashby, M.F. (1982) "Deformation Mechanisms Maps: The Plasticity and Creep of
277 Metals and Ceramics". 1st ed., Pergamon, Oxford; New York; Sydney.

278 Frost, B.R. (1991) Introduction to oxygen fugacity and its petrologic importance, in
279 "Reviews in Mineralogy" Volume 25, *Oxide Minerals: Petrologic and Magnetic*
280 *Significance*, D. H. Lindsley Ed., Mineralogical Society of America, New York, pp. 1-10.
281 Girard, J. Chen, J., Raterron, P., Holyoke, C.W. III (2013) Hydrolytic weakening of olivine at
282 mantle pressure: evidence of [100](010) slip system softening from single crystal
283 deformation experiments, *Physics Earth Planet. Int.* **216**, 12-20.
284 Hansen, L.N., Zimmerman, M.E., Kohlstedt, D.L. (2011) Grain boundary sliding in San
285 Carlos olivine: Flow law parameters and crystallographic-preferred orientation, *Journal of*
286 *Geophysical Research* **116**, B08201, doi:10.1029/2011JB008220.
287 Hansen, L.N., Zimmerman, M.E., Kohlstedt, D.L. (2013) Laboratory measurements of
288 viscous anisotropy of olivine aggregates, *Nature* **492**, 415-418.
289 Herd, C.D.K. (2008) Basalts as probes of planetary interior redox state, *Rev. Mineral.*
290 *Geochem.* **68**, 527–553.
291 Hilairet, N., Wang, Y., Sanehira, T., Merkel, S., Mei, S. (2012) Deformation of olivine under
292 mantle conditions: An in situ high-pressure, high-temperature study using monochromatic
293 synchrotron radiation *Journal of Geophysical Research* **117**, B01203, doi:
294 10.1029/2011JB008498.
295 Hiraga, T., Miyazaki, T., Tasaka, M., Yoshida, H. (2010) Mantle superplasticity and it self-
296 made demise, *Nature* **468**, 1091-1094, doi: 10.1038/nature09685.
297 Hirth, G., Kohlstedt, D.L. (1995) Experimental constraints on the dynamics of partially
298 molten upper mantle 2: deformation in the dislocation creep regime, *Journal of*
299 *Geophysical Research* **100**, B8, 15441-15449.
300 Hirth, G., Kohlstedt, D.L. (2003) Rheology of the upper mantle and the mantle wedge: a view
301 from the experimentalists, in: Inside the Subduction Factory, *Geophys. Monogr. Ser.* **138**,
302 J. Eiler (Ed.), AGU, Washington, D. C., pp. 83–105.
303 Keefner, J.W., Mackwell, S. J., Kohlstedt, D. L., Heidelbach, F. (2011) Dependence of
304 dislocation creep of dunite on oxygen fugacity: implications for viscosity variations in
305 Earth's mantle, *Journal of Geophysical Research* **116**, B05201, doi:
306 10.1029/2010JB007748.
307 Kohlstedt, D.L. (2006) The role of water in high-temperature rock deformation, *Reviews in*
308 *Mineralogy & Geochemistry* **62**, 377-396.
309 Mackwell, S.J., Kohlstedt, D.L., Paterson, M.S. (1985) The role of water in the deformation
310 of olivine single crystals, *Journal of Geophysical Research* **90**, 11319-11333.

311 Ohuchi, T., Kawazoe, T., Higo, Y., Suzuki, A. (2017) Flow behavior and microstructures of
312 hydrous olivine aggregates at upper mantle pressures and temperatures, *Contrib. Mineral.*
313 *Petrol.* **172**:65, doi: 10.1007/s00410-017-1375-8.
314 Raterron, P., Wu, Y., Weidner, D.J., Chen, J. (2004) Low temperature olivine rheology at
315 high pressure, *Phys. Earth Planet. Int.* **145**, 149-159, doi:10.1016/j.pepi.2004.03.007.
316 Raterron, P., Amiguet, E., Chen, J., Li, L., Cordier, P. (2009) Experimental deformation of
317 olivine single crystals at mantle pressure and temperature, *Phys. Earth Planet. Int.* **172**, 74-
318 83.
319 Raterron, P., Girard, J., Chen, J. (2012) Activities of olivine slip systems in the upper mantle,
320 *Phys. Earth Planet. Int.* **200-201**, 105-112.
321 Skemer, P., Sundberg, M., Hirth, G., Cooper, R. (2011) Torsion experiments on coarse-
322 grained dunite: implications for microstructural evolution when diffusion creep is
323 suppressed, Geological Society, London, Special publication 360, 211-233,
324 doi:10.1144/SP360.12 .
325 Tielke, J.A., Hansen, L.N., Tasaka. M., Meyers, C., Zimmerman, M.E., Kohlstedt, D.L.
326 (2016) Observation of grain size sensitive power law creep of olivine aggregates over a
327 large range of lattice-preferred orientation strength, *J. Geophys. Res. Solid Earth* **121**, 506-
328 516, doi:10.1002/2015JB012302.
329 Turcotte, D.L., Schubert, G. (2002) "*Geodynamics"*, Second Ed., Cambridge University
330 Press, NY, USA, pp. 456.
331 Warren, J.M., Hirth, G. (2006) Grain size sensitive deformation mechanisms in naturally
332 deformed peridotites, E*arth and Planetary Sciences Letters* **248**, 438-450.
333 Wendland, R.F., Huebner, J.S., Harrison, W.J. (1982) The redox potential of boron nitride and
334 implications for its use as a crucible material in experimental petrology, *American*
335 *Mineralogist* **67**, 170-174.
336
337

338 **Acknowledgements**

339 This research was supported by the Agence Nationale de la Recherche (ANR) Grant
340 BLAN08-2_343541 “Mantle Rheology”. We thank two anonymous reviewers for their
341 thoughtful insights which helped improving the original manuscript. Part of the work was
342 carried out while PR was serving at the National Science Foundation.

Figure 1: Schematics of mechanisms accommodating strain in olivine aggregates: dislocations (blue corners) glide, cross slip and climb within grains, disclinations (blue spirals, *Cordier et al.* [2014]) mostly active near grain boundaries, ionic diffusion (red arrows) occurring at grain interfaces (Cobble diffusion) or within the grains (Nabarro-Herring diffusion, dislocation climb), and grain-boundary sliding (green arrows, *Hansen et al.* [2011]) which also involves diffusion and can be assisted by dislocations. Other mechanisms that do not accommodate strain, such as grain-boundary migration or recrystallization, also assist olivine deformation.

Figure 2: A) Aggregate strain rate $\dot{\varepsilon}_{\mathrm{Agg}}$ as measured in experiments (Table S1) versus predictions based on intracrystalline strain rate $\dot{\varepsilon}_{\mathrm{IC}}$ as calculated from Eq. 3 and Table S2 parameters. The color code indicates experimental temperatures. D, H, and B are data from Durham et al. [2009], Hilairet et al. [2012], and Bollinger et al. [2013], respectively. Also show are the data reported by Tielke et al. [2016] (T; open diamond, green is for 1523K): for these data, shear strain rates and stresses were converted into compressional strain rates and stresses. The thick black line is identity, for which both strain rates are equal. Dotted and dashed lines indicate ratios for which the aggregate strain rate is 4.6 (dotted black), 19 (red), 63 (orange), 281 (blue), and 1995 (dashed black) times faster than the intracrystalline strain rate. B) $\log\left(\dot{\varepsilon}_{\mathrm{Agg}}/\dot{\varepsilon}_{\mathrm{IC}}\right)$ versus experimental differential stress; the colored lines are the results of a bilinear fit in T and σ through the data (Eq. 4); their color indicate temperature.

Figure 3: A) ratio of the aggregate strain rate by the intracrystalline strain rate ($\dot{\varepsilon}_{Agg}/\dot{\varepsilon}_{IC}$) versus depth, as calculated from Eq.4 assuming no effect of grain size, along 20-Ma (red) and 80-Ma (orange) oceanic geotherms, and a continental geotherm (blue) with a differential stress σ = 1 MPa (solid lines) and 50 MPa (dashed line). B) Olivine aggregate dynamic viscosity as calculated along a 20-Ma oceanic geotherm (red lines) and a continental geotherm (blue lines) at 1 MPa stress and indicated conditions. The solid lines were obtained from Eq.5 assuming wet conditions. The aggregate intracrystalline strain rate ($\dot{\varepsilon}_{IC}$) is showed for comparison (Intracrystalline). Previously reported high-temperature and low temperature flow laws for olivine polycrystals are also shown for comparison: H&K03 stands for *Hirth and Kohlstedt* [2003] dislocation creep law, assuming an activation volume of 12.8 cm^3/mol and an hydroxyl content C_{OH} = 300 ppm H/Si. Dem13 stand for *Demouchy et al.* [2013], and Rate04 for *Raterron et al.* [2004]. See text for further explanation. The effect of intergranular strain relaxation mechanism is apparent through the reduction of viscosity by a factor of ~100 (solid lines) at shallow depths relative to that obtained from the classical *Hirth and Kohlstedt*'s flow laws or laws based on intracrystalline deformation (dashed lines). Do note, however, that such effect is probably reduced in the mantle because of larger grain sizes than in experiments. At deeper depths, the difference between the present law and that of *Hirth and Kohlstedt* [2003] is due to the pressure-induced change of dominant slip system in olivine.

382 **Figure 1**

383

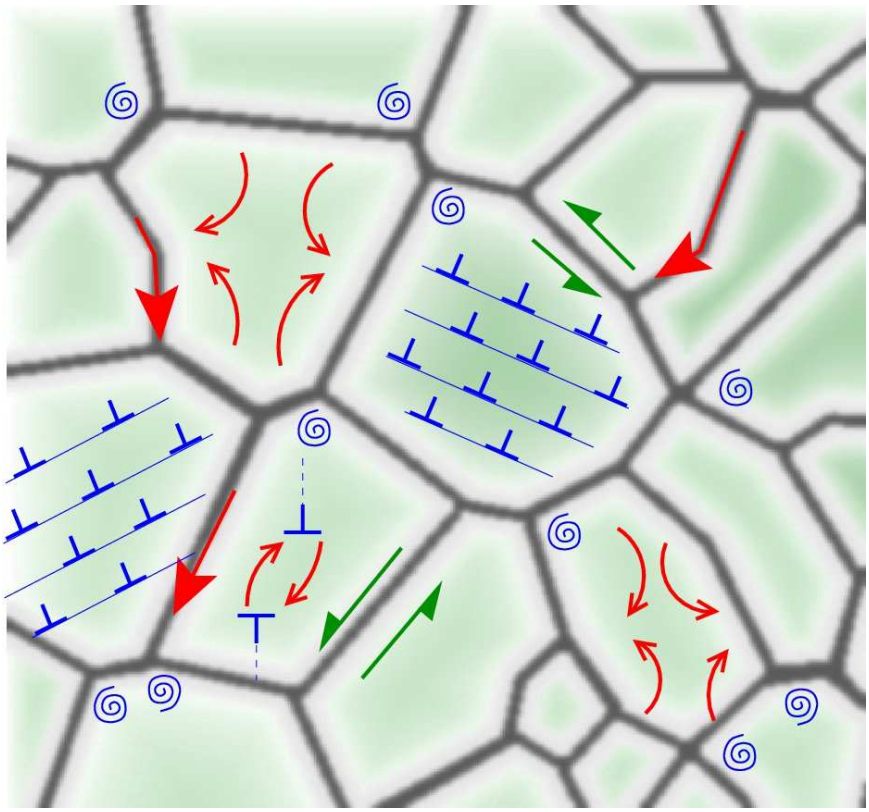

384

Figure 2.a

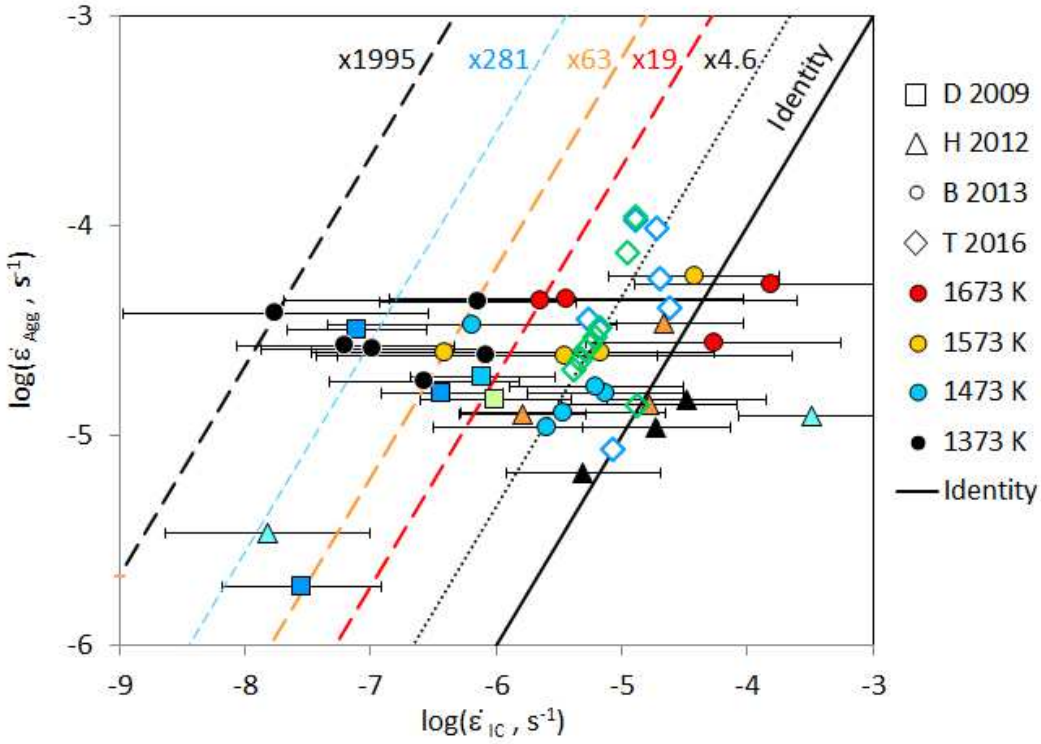

Figure 2.b

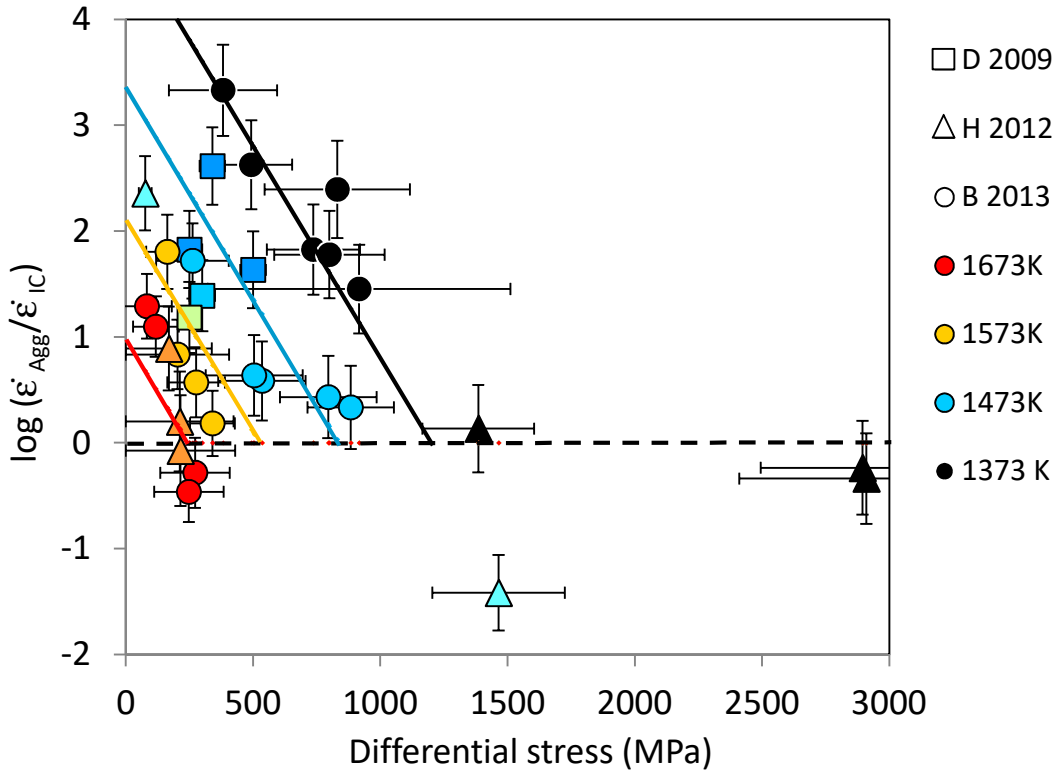

Figure 3.a

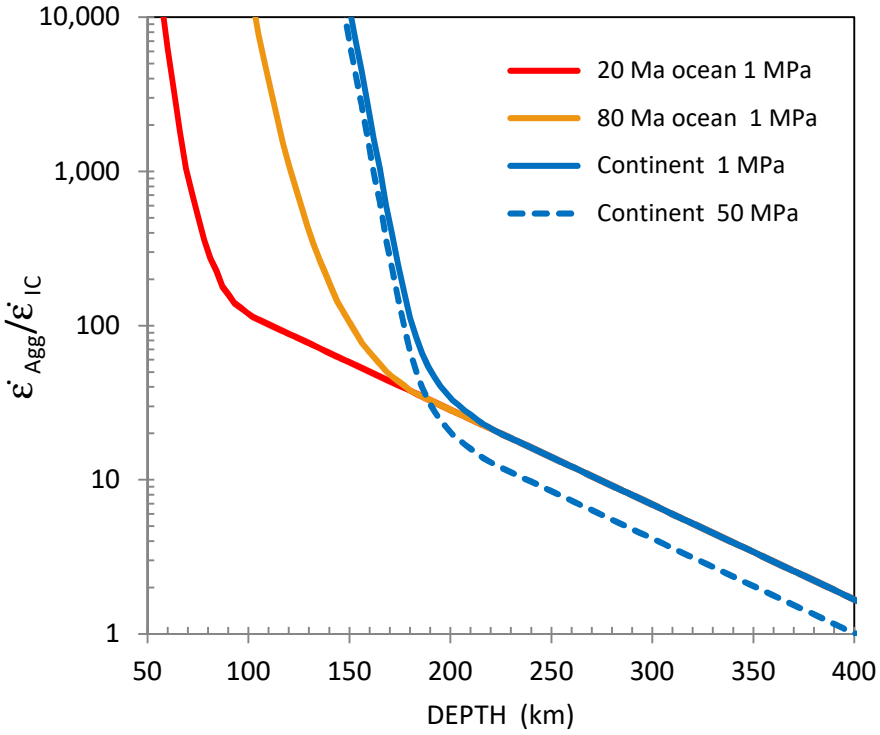

Figure 3.b